Short-time-scale variability in ventilation and export productivity during the formation of Mediterranean sapropel S1

Tom Jilbert,[1] Gert-Jan Reichart,[1,2] Paul Mason,[1] and Gert J. de Lange[1]

Received 12 March 2010; revised 10 August 2010; accepted 18 October 2010; published 31 December 2010.

[1] High-resolution laser ablation–inductively coupled plasma–mass spectrometry (LA-ICP-MS) scanning of laminated sediments from the Urania basin is used to investigate short-time-scale variability in export productivity and redox conditions during the formation of eastern Mediterranean sapropel S1. Sedimentary enrichments of molybdenum (Mo), vanadium (V), and uranium (U) reflect deep-water redox conditions, most likely those near to the seawater-brine interface, while enrichment of Ba is related to biogenic barite and hence to export productivity. The enrichments of all four elements show strong variability on multidecadal to multicentennial time scales throughout S1. A partial decoupling of export productivity from redox conditions at the height of sapropel formation suggests that hydrographic changes, i.e., a variable ventilation rate of the eastern Mediterranean, played an important role in determining deep-water redox conditions. A pronounced switch is observed in the enrichments of redox-sensitive trace metals, from dominantly 300–600 year variability during early S1 to dominantly 100–300 year variability during late S1, indicating a change in the mean frequency of variability in the ventilation rate. The presence of a similar shift in the frequency of tropical and extratropical climate records at this time suggests that ventilation of the eastern Mediterranean was coupled to global climate variability.

Citation: Jilbert, T., G.-J. Reichart, P. Mason, and G. J. de Lange (2010), Short-time-scale variability in ventilation and export productivity during the formation of Mediterranean sapropel S1, *Paleoceanography*, *25*, PA4232, doi:10.1029/2010PA001955.

1. Introduction

[2] Few phenomena in the marine sediment record have been studied so thoroughly as the sapropels of the eastern Mediterranean. These highly conspicuous organic-rich layers, which punctuate the hemipelagic marls of Mediterranean sediment cores and land sections, have attracted paleoclimatologists from a wide range of disciplines since the pioneering work of *Olausson* [1961]. As a consequence, it is now well established that sapropels form rhythmically, in association with northern hemisphere insolation maxima driven by orbital precession [*Hilgen* 1991; *Rossignol-Strick*, 1985], and have done so since the Miocene [*Cita and Grignani*, 1982; *Lourens et al.*, 1996; *Thunell et al.*, 1984].

[3] During sapropel formation, an intensified African monsoon enhances Nile outflow [*Rossignol-Strick et al.*, 1982], and activates dormant river systems elsewhere in North Africa [*Rohling et al.*, 2002a]. Precipitation in southern Europe increases simultaneously [*Bard et al.*, 2002; *Kotthoff et al.*, 2008; *Rohling and Hilgen*, 1991] due to an intensification of moisture transport in the westerlies band. The resulting altered hydrologic balance of the eastern Mediterranean triggers the formation of organic-rich sediments, although a number of mechanisms may be involved. Evidence has been presented for enhanced export productivity during sapropels [*Calvert*, 1983; *de Lange and ten Haven*, 1983; *Passier et al.*, 1999]. This implies an increased supply of limiting nutrients to the photic zone, either by enhanced river runoff, or, in the case of phosphorus, enhanced regeneration from the sediments [*Slomp et al.*, 2002], and in the case of nitrogen, fixation from the atmosphere [*Sachs and Repeta*, 1999]. The fraction of carbon exported to the deep waters may be enhanced by the presence of a deep-chlorophyll maximum [*Rohling and Gieskes*, 1989] characterized by inefficient carbon recycling. On the other hand, changes in water buoyancy and circulation have been shown to isolate deep-water masses during sapropel formation [*Rohling*, 1994; *Rohling and Bryden*, 1994] and hence precondition the eastern Mediterranean for suboxia or anoxia, which may in turn intensify under elevated export productivity levels. Such deep-water sub/anoxia enhances the preservation of exported organic matter [see *de Lange et al.*, 2008] providing an additional mechanism for carbon enrichment in the sediments.

[4] Due to the sampling resolution of most studies, conclusions on the stability of the conditions leading to sapropel formation, or coupling between export productivity and the deep-water redox state, are largely based on centennially averaged data. Many sapropel sediments also show some evidence of syndepositional or postdepositional bioturbation, limiting their use as high-resolution archives for comparison with other regional and global records. Several studies have identified single multicentennial "interrup-

[1]Department of Earth Sciences–Geochemistry, Faculty of Geosciences, Utrecht University, Utrecht, Netherlands.
[2]Alfred Wegener Institute for Polar and Marine Research, Biogeosciences, Bremerhaven, Germany.

0883-8305/10/2010PA001955

tions" within sapropels [e.g., *Kotthoff et al.*, 2008; *Mercone et al.*, 2001; *Meyers and Arnaboldi*, 2005; *Rohling et al.*, 2002a], which have been interpreted as large-scale ventilation events triggered by millennial-scale climate variability in the northern hemisphere [*Rohling et al.*, 2002b]. Furthermore, observations of oxyphilic benthic formaminifera in sapropels from the Aegean Sea and offshore Libya [*Casford et al.*, 2003] have raised the possibility that less intense but more frequent interruptions may occur throughout sapropel deposition. However, the precise duration of such events, and the roles in their occurrence of export productivity and physical ventilation changes, remain to be established. Improving the resolution of export productivity and redox proxy profiles within sapropels may hold the key to identify the processes controlling these events, and how they relate to climate variability on a global scale.

[5] Here we investigate short-time-scale export productivity and redox variability during the most recent sapropel, S1, using geochemical proxies. We first establish the oceanographic and geochemical mechanisms responsible for short-time-scale variability in the enrichments of barium (Ba), molybdenum (Mo), vanadium (V) and uranium (U). Subsequently, we investigate the potential climatic drivers of these mechanisms. The early Holocene interval during which S1 was deposited is represented in high-resolution terrestrial climate records from a range of latitudes [e.g., *Bar-Matthews et al.*, 2003; *Fleitmann et al.*, 2003; *Mayewski et al.*, 1997].

2. Marine Geochemistry of Ba, Mo, V, and U in the Context of Sapropel S1

[6] Enrichment of Ba in sapropel sediments is traditionally thought to be caused by the preservation of barite ($BaSO_4$), which precipitates within decaying organic matter during its descent through the water column [*Bishop*, 1988; *Dehairs et al.*, 1980]. Due to the close correspondence of sedimentary Ba and organic carbon enrichments in unoxidized sapropels, the magnitude of this "biogenic"-Ba enrichment has been proposed to reflect export productivity (i.e., the organic-carbon flux to the seafloor) during sapropel formation [e.g., *Pruysers et al.*, 1991; *Thomson et al.*, 1995; *van Santvoort et al.*, 1996]. However, a number of potential caveats are associated with the use of sedimentary barite enrichments for reconstructions of export productivity (see review of *Paytan and Griffith* [2007]). First, changes in the ambient dissolved-Ba concentration may lead to variable precipitation rates of barium in the water column [*Dymond et al.*, 1992], or variable dissolution rates of biogenic barite in the water column and at the sediment-water interface [e.g., *Eagle et al.*, 2003; *McManus et al.*, 1998]. Second, barite may dissolve after deposition if pore waters become sulfate-depleted [e.g., *van Os et al.*, 1991]. *McManus et al.* [1998] also provide evidence for regeneration of dissolved Ba from coastal margin sediments which show no significant depletion of pore water sulfate, suggesting that (labile) solid-phase species other than barite may be quantitatively important in the marine Ba cycle. Finally, in locations where the biogenic barite enrichment is low, changes in the detrital Ba/Al ratio may become significant if normalization to Al is used to estimate Ba enrichment [*Reitz et al.*, 2004].

[7] Enrichments of Mo, V and U in sapropel sediments have been interpreted to reflect changing water column redox conditions during sapropel formation [*Arnaboldi and Meyers*, 2007; *Gallego-Torres et al.*, 2010; *Mercone et al.*, 2001; *Nijenhuis et al.*, 1999; *Warning and Brumsack*, 2000]. The most commonly observed mechanism for sedimentary Mo, U and V enrichment in modern low oxygen environments is reductive transformation of the oxyanions MoO_4^{2-}, $UO_2(CO_3)_3^{4-}$ and $H_2VO_4^-$ into stable solid phase species, either at, or by diffusion across, the sediment water interface [e.g., *Crusius et al.*, 1996; *Emerson and Huested*, 1991]. Such transformations occur when the reduction potential (E_h) of pore waters decreases to critical values, as electron acceptors are used in organic matter remineralization. Pourbaix diagrams predict reductive precipitation of the three metals to occur close to the E_h level of iron oxide reduction, in the order U → V → Mo with decreasing E_h (Figure 1a, note simplified ion systems). Field and experimental evidence also suggests that the reduction of all three elements to insoluble forms may be accelerated in the presence of free sulfide [*Helz et al.*, 1996; *Klinkhammer and Palmer*, 1991; *Wanty and Goldhaber*, 1992]. This appears to be particularly important for Mo; the oxyanion MoO_4^{2-} undergoes rapid transformation to particle-reactive oxythiomolybdates during reaction with HS^-, a phenomenon known as the "sulfide switch" [*Helz et al.*, 1996]. MoO_4^{2-} in oxic seawater also associates with iron and manganese oxides, hence Mo may be shuttled to the sediments by these carrier phases [e.g., *Crusius et al.*, 1996], but will be released as they dissolve in suboxic conditions [*Brumsack*, 2006; *van der Weijden et al.*, 2006]. Whatever the mechanism of trace metal removal to the sediments, persistent stagnation of water masses can also result in the depletion of MoO_4^{2-}, $[UO_2(CO_3)_3]^{4-}$ and $H_2VO_4^-$ [see *Colodner et al.*, 1995; *Emerson and Huested*, 1991], potentially decreasing the rate of subsequent removal to the sediments by means of the "basin reservoir effect" [*Algeo and Lyons*, 2006].

3. Materials and Methods

3.1. Study Location

[8] Piston Core PP44PC (35°14.20 N, 21°29.80 E) was recovered from 3400 m depth, within the Urania basin in the eastern Mediterranean (Figures 1b and 1c). The basin is a depression within the so-called "cobblestone topography" of the Mediterranean Ridge accretionary wedge [*Kastens*, 1981], and is filled with a brine of major ionic ratios similar to those of seawater, but with roughly six times higher salinity (Table 1). A number of such brine-filled basins have been discovered on the Mediterranean Ridge; their occurrence is related to the compressional deformation, and subsequent dissolution, of Messinian evaporite strata in the subsurface [*Camerlenghi*, 1990], or the consequent upward motion of relic brine [*Vengosh et al.*, 1998]. Although the strength and major-ion composition of the brines vary between basins, all display a strongly stratified seawater-brine interface, coincident with a steep E_h gradient from seawater oxygen concentrations to complete anoxia over

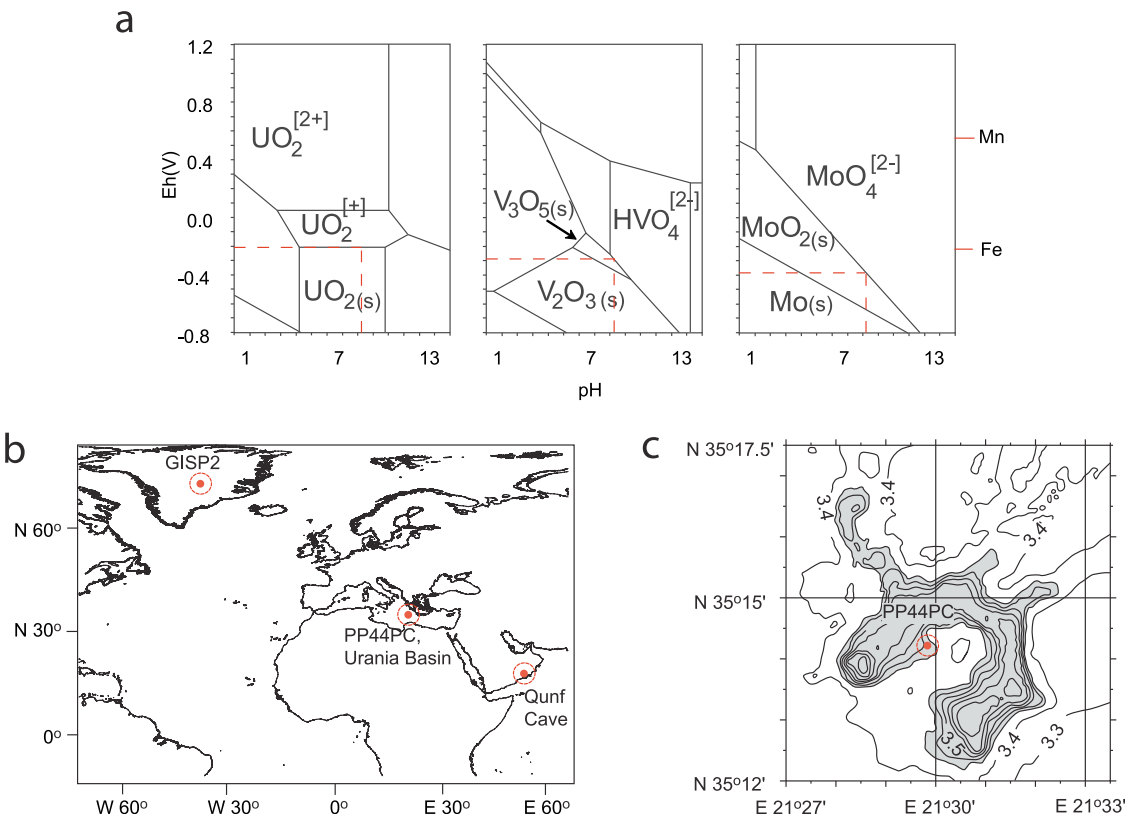

Figure 1. (a) Pourbaix E_h-pH diagrams for U, V, and Mo, as calculated from the FACT thermodynamic database with the software FACTSAGE [*Bale et al.*, 2002], redrawn from *Takeno* [2005] with permission. The diagrams represent the simple system Element-H-O at a total solute concentration of 10^{-10} mol kg^{-1}, standard temperature and pressure, thus simplifying the true dynamics of eastern Mediterranean seawater during sapropel formation. Dashed lines indicate E_h precipitation thresholds at seawater pH (8.2). The reductive precipitation thresholds of Mn and Fe oxides under the same conditions are shown to the right. (b) Map showing the coring site of PP44PC in the Urania basin, eastern Mediterranean, and locations of contemporaneous climate records used in this study. (c) Bathymetric detail of the Urania basin, with depth contours in kilometers. Contour interval is 0.1 km outside the basin and 0.02 km inside the basin. Shaded area indicates brine surface.

less than a meter [*de Lange et al.*, 1990a]. Unfortunately, no data exist for Mo, U and V concentrations in the Urania brine. However, concentrations of Mo, U and V in the brines of the Bannock and Tyro basins show strong depletions across the seawater-brine interface. Concentrations of Mo and U decrease to values below the detection limit of the neutron activation analysis technique employed by *van der Weijden et al.* [1990], while the concentration of V drops to roughly 0.25 times the value in the overlying seawater (Table 1) [*van der Weijden et al.*, 1990]. Such strong depletions are consistent with the reducing nature of the brines, and are also expected to be present in the Urania basin, which has the highest sulfide content of any of the basins yet discovered (Table 1).

3.2. Discrete Sampling and Dating

[9] The S1 interval in PP44PC is finely laminated and visibly distinct from the rest of the core by its olive green

Table 1. Concentrations of Dissolved Constituents in Eastern Mediterranean Brine Basins and Typical Seawater Values[a]

Brine	Na	Cl	Mg	K	Ca	SO_4	HS	CH_4	Ba	Mo	U	V
Urania	3503	3729	316	122	32	107	16	5.56	-	-	-	-
Bannock	4235	5360	650	127	17	137	3.0	0.45	290	<20	<2	6.7
Seawater	528	616	60	11.4	11.6	31.8	2.6×10^{-6}	1.5×10^{-6}	50–150	160	16	32

[a]All values in mmol/L except for Ba (nmol/L) and Mo, U, and V (μmol/L). All data from *van der Wielen et al.* [2005], except Ba [from *de Lange et al.*, 1990b] and Mo, U, and V [from *van der Weijden et al.*, 1990].

color. Discrete samples were taken from the S1 interval at 3 mm resolution, freeze-dried, ground and analyzed for major and minor element concentrations by inductively coupled plasma–atomic emission spectroscopy (ICP-AES) (instrumental precision better than 5%), Organic carbon (C_{org}) content was analyzed on selected samples by thermal combustion elemental analysis (TCEA) after decalcification in 1M HCl (instrumental precision better than 3%). Age control within the S1 interval was established by AMS ^{14}C dating of the organic-carbon residue of four samples, corrected to calendar years B.P. after calibration to the Marine04 curve [*Hughen et al.*, 2004] (Figure 2c). The variable global reservoir age calculated by the ocean-atmosphere diffusion model of Marine04 was assumed, with no regional offset (i.e., $\Delta R = 0$), as shown to be valid for the modern Mediterranean [*Siani et al.*, 2000]. The age model was constructed using a linear best fit through the four dates, which falls within the 1-sigma uncertainty of each. The calculated sedimentation rate is 6.06 cm/kyr, corresponding to a discrete sampling resolution of 49.5 years (3 mm). The linearity of the sedimentation rate suggests that variability in ΔR between the four sampling intervals [see *Siani et al.*, 2001] was negligible.

3.3. Resin Embedding and LA-ICP-MS

[10] Across the S1 interval, sediment blocks were excavated in aluminum trays from the core surface, resin-embedded in a nitrogen-filled glove box [*Jilbert et al.*, 2008] and polished. Major, minor and trace elements, including Ba, Mo, V, U and Al, were analyzed by LA-ICP-MS scanning. Each block was mounted on a stage within a sealed ablation chamber. A 193 nm Lambda Physik excimer laser beam (pulse repetition rate 10 Hz, diameter 80 μm, energy density 8 Jcm^{-2}) was focused onto the sample, and ablated material was transported on He-Ar carrier gas to a quadrupole ICP-MS (Micromass Platform, measurement frequency 50 Hz). The stage was set in steady motion to create an ablation trace perpendicular to the laminations within the sapropel. The combination of measurement frequency and stage speed yields data points separated by ~20 μm, with each point representing all the material ablated over each 20 μm increment of the stage motion. Due to the 80 μm diameter of the laser beam target, each point thus represents an average of a 100 μm interval. The sedimentation rate of 6.06 cm/kyr results in a LA-ICP-MS data resolution of 1.65 years (100 μm). Ion counts for each element were measured on specific isotopes to avoid mass overlap (Table 2). Repeat measurements of the standard material NIST610, before and after each sample trace, allowed instrumental precision for each element to be estimated (Table 2). Because ablation rate during LA-ICP-MS is nonconstant, precision estimates are made relative to a selected isotope (in this case ^{44}Ca). To generate approximate concentration data, all LA-ICP-MS ion counts were corrected for background values in the carrier gas, for inter-element fractionation effects by reference to the fractionation coefficients (ion counts/ppm) of NIST610, and for the natural abundance of the measured isotope with respect to all isotopes of the element in question. Element/Al ratios were then calculated from these corrected values.

3.4. Statistical Analysis of Time Series Data

[11] Time series of LA-ICP-MS-derived element/Al enrichments from this study, and existing high-resolution climate records from the literature, were spectrally decomposed by means of Morlet wavelet analysis, using the online software of C. Torrence and G. P. Compo (http://ion.researchsystems.com/IONScript/wavelet/) [*Torrence and Compo*, 1998]. Prior to analysis, the 6700–10900 B.P. interval was selected from each series, low-pass filtered at a cutoff of 30 years, detrended and normalized to unit variance. For further analysis of the LA-ICP-MS element/Al time series, periodicity bands of elevated spectral power were identified from the corresponding wavelet spectra. The series were band-pass filtered at these periodicities, and running correlations were performed on pairs of band-pass-filtered series using a window and step size appropriate to the band pass. The running correlation procedure effectively calculates the coherence between two series (i.e., the covariance at a specified frequency, independent of the power of that frequency in the wavelet).

4. Results and Discussion

4.1. Proxy Preservation

[12] A positive linear correlation is observed between Ba/Al and C_{org} in the discrete sample series of sapropel S1 in PP44PC (Figure 2b), implying that the Ba enrichment in sapropel S1 sediments at this location is indeed related to biogenic barite, and that sedimentary barite provides a reliable estimate of the organic carbon flux to the seafloor. The magnitude of the Ba enrichment is greatly in excess of the detrital background for the eastern Mediterranean (close to the global average shale value of 0.0037, Figure 2a), indicating that normalization to Al offers a valid measure for biogenic barite enrichment. Furthermore, the sulfate content of the Urania brine is 107 mmol/L, roughly 3.5 times the seawater value (Table 1), preventing barite dissolution by undersaturation. However, these observations do not exclude the possibility that the relationship between export productivity and primary productivity (the f ratio [*Laws et al.*, 2000]) may have varied during S1; hence, the Ba/Al data must be discussed strictly in terms of carbon fluxes to the seafloor (export productivity), and not primary productivity (see *Eagle et al.* [2003] for further discussion).

[13] The close correspondence between Ba/Al and C_{org} in the uppermost part of S1 (Figure 2a) confirms that postdepositional oxic "burn-down" of S1 [*van Santvoort et al.*, 1996] did not occur, consistent with an interpretation of persistent anoxic brine conditions in the Urania basin throughout the Holocene [*Hübner et al.*, 2003]. This implies that no remobilization of redox-sensitive trace metals such as Mo, V and U has taken place due to the propagation of a burn-down front [see *Thomson et al.*, 1995].

4.2. General Characteristics of LA-ICP-MS Profiles

[14] The Al-normalized LA-ICP-MS profiles of Ba, Mo, V and U (Figure 2c) show that all four elements are enriched in the S1 interval in PP44PC, relative to global average shale values. The magnitudes of the mean enrichments of Mo, V and U (and the first-order shapes of the profiles) are

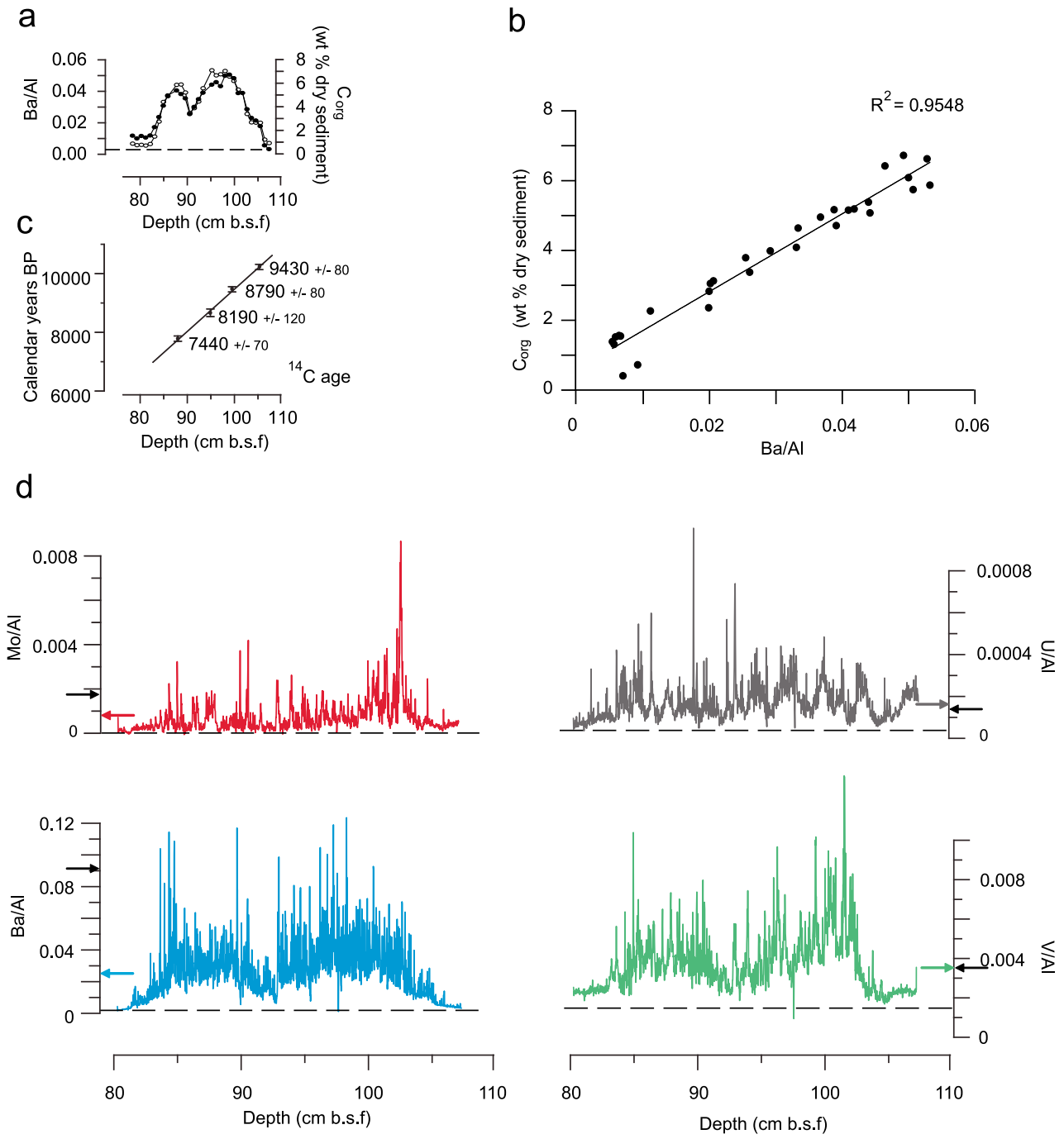

Figure 2. (a) Comparison of discrete-sample Ba/Al (open circles) with C_{org} (in weight %, filled circles) through the S1 interval in PP44PC. Horizontal dashed line represents global mean shale value of Ba/Al [*Turekian and Wedepohl*, 1961]. Note that data resolution is lower than the 3 mm core-sampling resolution because C_{org} analysis was not performed on all samples. b.s.f, below seafloor. (b) An x-y plot of the same data. (c) Radiocarbon dating of S1 in PP44PC. Dates are reported as calendar years B.P. after calibration to the Marine04 curve [*Hughen et al.*, 2004]. The age model was constructed using a linear best fit through the four points, which falls within the 1-sigma uncertainties of all points (vertical error bars). Raw ^{14}C ages indicated alongside data points. b.s.f, below seafloor. (d) Five-point running means of 20 μm resolution LA-ICP-MS scan data, plotted as element/Al after corrections described in section 3. Horizontal dashed lines represent global mean shale values [*Turekian and Wedepohl*, 1961]. Arrows inside vertical scales represent mean values of the complete series. Arrows outside vertical scales represent mean values in S1 in core LC21 [*Mercone et al.*, 2001]. b.s.f, below seafloor.

Table 2. Isotopes Measured by LA-ICP-MS, and Precision Relative to ^{44}Ca as Estimated by Repeat Analysis of Standard Material NIST610

	Element											
	Na	Mg	Al	K	Ca	Ca	Ti	V	Mn	Fe	Co	Ni
Isotope	23	24	27	39	43	44	49	51	55	57	59	60
Precision (%)	3.4	3.4	6.9	1.8	0.8	-	3.6	2.0	1.4	1.3	1.7	3.2
	Element											
	Cu	Zn	Sr	Zr	Mo	Mo	Cd	Cd	Ba	Ba	Pb	U
Isotope	65	66	88	90	97	100	111	114	137	138	208	238
Precision (%)	4.7	4.0	3.17	9.1	1.2	1.1	8.1	9.1	2.1	2.3	9.1	11.9

similar to those observed in the unoxidized sapropel S1 interval from a core in the SE Aegean Sea [*Mercone et al.*, 2001]. This observation is important as it implies that the source of the Mo, V and U enrichments in PP44PC is not specifically related to the Urania brine, although the brine may have been instrumental in subsequent preservation of the signals. The profiles of all four elements show some common features on the (multi)millennial scale, most notably the twin Gaussian structure dividing the sapropel into "early S1" and "late S1" intervals, with a saddle of low enrichments defining "mid-S1." This correspondence suggests that the carbon flux to the seafloor, and the severity of reducing conditions at the location of trace metal precipitation, broadly covaried on the (multi)millennial scale. However, on shorter time scales, the relationships between the enrichments of each element become more complex. Wavelet spectra of the LA-ICP-MS data confirm the existence of quasi-cyclic, multicentennial and multidecadal time scale variability in the enrichments of all four elements (Figure 3). Three useful arbitrary periodicity bands may be defined based on the results, namely, 300–600 years, 100–300 years and 30–100 years.

4.3. Patterns of Multicentennial and Multidecadal Variability in Elemental Enrichments

[15] High power in the multicentennial bands (300–600 years, 100–300 years) is observed in the wavelet spectra of all four elemental enrichments (Figure 3). A pronounced switch from dominantly 300–600 year to dominantly 100–300 year variability is observed in U/Al at ~9 kyr B.P. This switch is also evident in V/Al, but its significance is damped by high power in the 30–100 year band throughout the V/Al profile. Damping of power in the multicentennial frequencies appears to be even greater in the case of Mo/Al, which is strongly dominated by 30–100 year variability throughout S1. Ba/Al shows intermittent high power in the 100–300 year band throughout S1, and an interval of high power in the 300–600 year band from ~10.0–8.5 kyr B.P. We band-pass filtered the LA-ICP-MS data at 300–600 years from 10700 to 9000 years B.P. (roughly defining "early S1"), and at 100–300 years from 9000 to 6700 years B.P. ("late S1"), in accordance with the switch in power in the wavelet spectra (Figure 4b). Running correlation analysis of these series shows strong positive coherence between U/Al and V/Al during late S1, but negative coherence during early S1 (Figure 4b). Ba/Al and V/Al show positive coherence, which is relatively strong at the onset and termination of S1, and during the mid-S1 saddle, and relatively weak at times of fully developed sapropel conditions in early S1 and late S1 (Figure 4b).

[16] High power in the multidecadal band (30–100 years) is observed in all elemental enrichments throughout S1, with the exception of U/Al during early S1 (Figure 3). Running correlation analysis of the 30–100 year band-pass-filtered series shows that V/Al and Mo/Al display strong positive coherence throughout S1 (Figure 4c). Ba/Al also shows positive coherence with both V/Al and Mo/Al. However, the strength of coherence is much greater during the onset and termination of S1, and during the mid-S1 saddle, than during the fully developed sapropel conditions of early S1 and late S1 (Figure 4c). This loss of coherence between Ba/Al and V/Al in early S1 and late S1 is even more pronounced than in the multicentennial band pass (compare Figures 4b and 4c).

4.4. Mechanisms of Redox-Sensitive Trace Metal Enrichment

[17] In most modern low-oxygen marine environments, redox-sensitive trace metal enrichment of the sediments occurs via diffusion of metal oxyanions across the sediment-water interface, and subsequent reductive precipitation [e.g., *Crusius et al.*, 1996; *Emerson and Huested*, 1991]. Several lines of evidence suggest that this mechanism cannot explain enrichments of Mo, U and V in the Urania basin, either today or during S1. The modern brine is highly sulfidic (Table 1) and is thought to contain similarly low concentrations of dissolved Mo, U and V as those observed at Bannock basin (Table 1). Thus, the reservoir of dissolved Mo, U and V from which precipitation at the sediment-brine interface can occur is limited. Theoretically, this situation could be maintained by diffusion of dissolved Mo, U and V across the seawater-brine interface, followed by rapid precipitation and settling to the sediments. However, in such a scenario, the steep concentration gradient across the seawater-brine interface would be expected to generate greater enrichments of Mo, U and V in the time since the S1 interval than during S1 deposition, due to the high concentrations of these elements in well ventilated, oxic seawater. Clearly, the opposite is true; i.e., a greatly enhanced flux of these elements to the sediments occurred during S1 (Figure 2c).

[18] Negligible enrichments of U and V were observed by *Tribovillard et al.* [2008] in modern anoxic sediments from the Orca brine basin in the Gulf of Mexico. These authors concluded that the long residence time of the brine (~5700 years) restricts the flux of U and V to the sediments, despite the favorable conditions for enrichment (the so-called "basin reservoir effect" [*Algeo and Lyons*, 2006]). The minimum residence time of the brine in the Bannock basin has been estimated, by analysis of its thermal structure, to be 4500 years [*Boldrin and Rabitti*, 1990]. Furthermore, the enriched and homogeneous $\delta^{18}O$ signal of the Bannock brine waters suggests that the brine formed during a glacial interval (thus, at the latest during the Younger Dryas, ~12000 years B.P.) and has not been significantly mixed since its formation

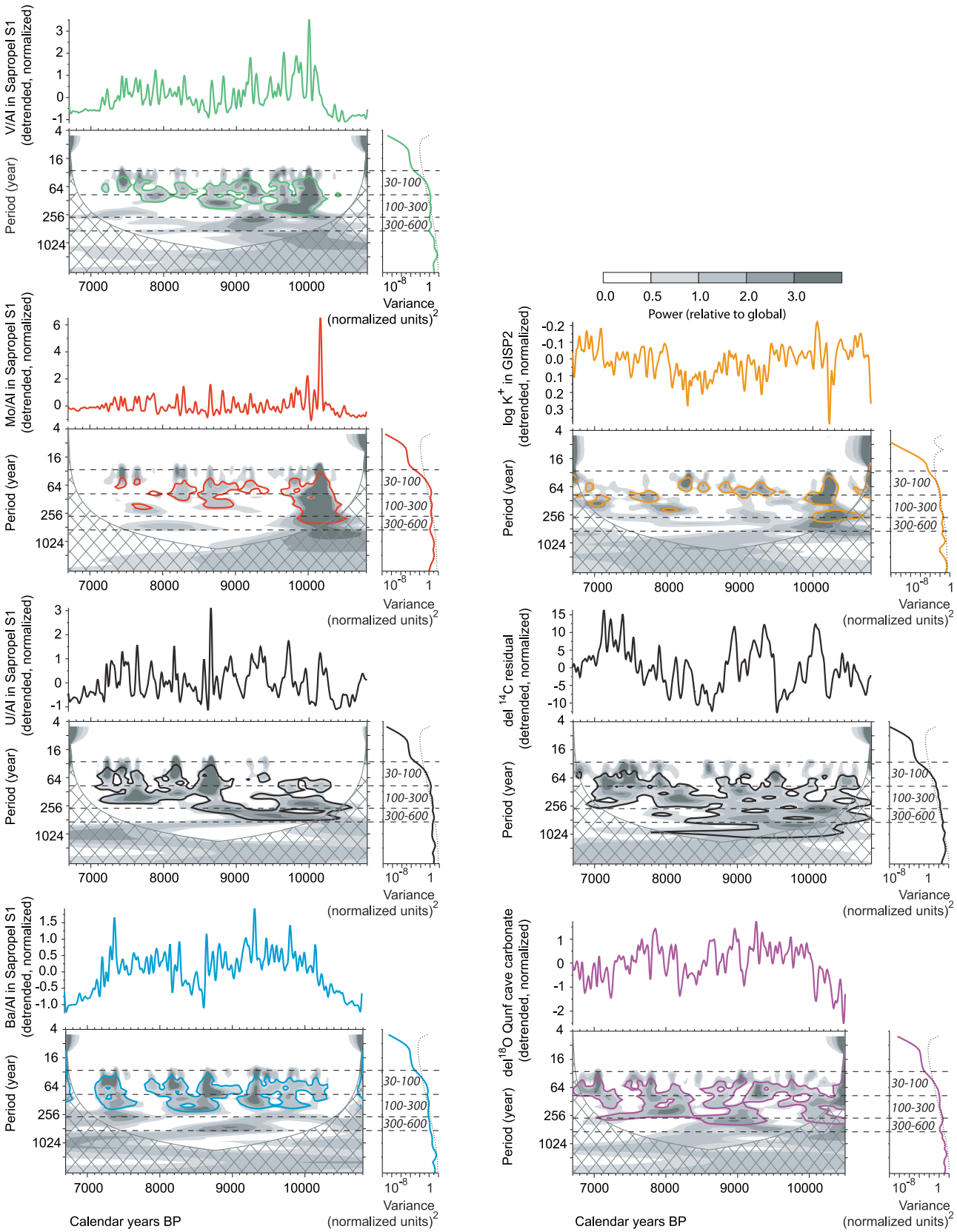
V/Al in Sapropel S1 (detrended, normalized)
Mo/Al in Sapropel S1 (detrended, normalized)
U/Al in Sapropel S1 (detrended, normalized)
Ba/Al in Sapropel S1 (detrended, normalized)
log K+ in GISP2 (detrended, normalized)
del 14C residual (detrended, normalized)
del 18O Qunf cave carbonate (detrended, normalized)
Period (year)
30-100
100-300
300-600
Variance (normalized units)2
0.0 0.5 1.0 2.0 3.0
Power (relative to global)
Calendar years BP

Figure 3

[*Stenni and Longinelli*, 1990]. *Hübner et al.* [2003] estimated the minimum age of the Urania brine to be ~6700 years B.P., and the well-preserved S1 interval in PP44PC suggests the basin could be much older still. This assimilated evidence points toward a residence time in the order of 10^3 years for the Urania brine, implying that the flux of trace metals to the sediments during nonsapropel conditions is probably limited by the basin reservoir effect, as in the Orca basin [*Tribovillard et al.*, 2008]. Indeed, Mo, V and U in PP44PC at the termination of S1 (~81 cm in Figure 2c) are not strongly enriched above global mean shale values, confirming that the enrichments during S1 do not appear to be related to direct precipitation from the Urania brine. A brine residence time in the order of 10^3 years also implies that the multidecadal to multicentennial variability in trace metal enrichments during S1 is not related to brine recharge on these time scales.

[19] The apparent passivity of the brine in regulating the enrichments of Mo, U and V during S1 suggests that precipitation of these metals took place either at the seawater-brine interface or in the overlying water column. Several studies have now established that seawater-brine interfaces act as loci for organic matter remineralization [e.g., *Sass et al.*, 2001; *van der Wielen et al.*, 2005], due to the accumulation of settling material at the density gradient [*Henneke and de Lange*, 1990; *Tribovillard et al.*, 2009]. Indeed, the residence time of organic material at the interface of the modern Orca brine is sufficient to allow extensive oxic degradation prior to sedimentation [*Tribovillard et al.*, 2009]. We propose that accumulation of degrading organic matter and other sediment components at the seawater-brine interface of the Urania basin provided the environment within which the oxyanions of Mo, U and V were reduced during S1 (Figure 5), similar to the trace metal-enriched "surficial fluff" of modern Black Sea sediments [*Crusius et al.*, 1996]. Such oxyanion reduction would be promoted, relative to today, by ambient suboxic conditions in the deep waters during S1 formation [*Reitz et al.*, 2006]. This mechanism appears more likely than precipitation in organic aggregates higher in the water column, due to the rapid settling of organic material during sapropel events [*Kemp et al.*, 1999]. We note that the association of V with organic matter in sequential extractions of S1 sediments supports the hypothesis that organic aggregates were the carrier phase of the precipitated metals to the seafloor [*Rutten and de Lange*, 2003]. Furthermore, the dissolution front of Mn oxides during S1 was situated at ~2000 km water depth, well above the Urania basin (3400m) [*de Lange et al.*, 2008; *Reitz et al.*, 2006], implying that Mn oxides were not involved in trace metal cycling in the deeper waters.

4.5. Controls on Redox Variability: Ventilation Versus Export Productivity

[20] The similarity of the magnitude and evolution of Mo, U and V enrichments in PP44PC with those elsewhere in the eastern Mediterranean [*Mercone et al.*, 2001], suggest a regional, rather than local, control on redox conditions near the Urania basin seawater-brine interface. However, both physical ventilation changes in the eastern Mediterranean, and a variable flux of organic carbon to the seawater-brine interface, may have influenced redox conditions in decaying aggregates accumulating at the density gradient (Figure 5). Furthermore, ventilation changes may also have altered the dissolved concentrations of Mo, U and V in the deep waters through an eastern Mediterranean-wide basin reservoir effect. The generally positive coherence between Ba/Al and the redox-sensitive trace metal enrichments at both multicentennial and multidecadal time scales (Figures 4b and 4c) implies that export productivity exerted some control on redox conditions near the seawater-brine interface, namely, that during times of higher carbon flux (and hence degradation), conditions were more reducing and the trace metal precipitation rate was higher. However, the correlation weakens during fully developed sapropel conditions in both early S1 and late S1, suggesting a partial decoupling of the two parameters. Especially in the 30–100 year band pass, no significant relationship exists between Ba/Al and either V/Al or Mo/Al for much of early S1 and late S1 (Figure 4c), despite the strong 30–100 year variability in all three elements (Figure 3). In contrast, V/Al and Mo/Al correlate strongly with each other throughout the 30–100 year band pass (Figure 4c).

[21] We interpret the partial decoupling of variability in Ba/Al from that of the redox-sensitive trace metal enrichments to represent an increasingly dominant role of variability in the deep-water ventilation rate (i.e., the inverse of deep-water residence time) in determining redox conditions at the seawater-brine interface. The most plausible mechanism for this effect is an increase in the amplitude of fluctuation of the ventilation rate at the height of sapropel conditions. A comparatively stable ventilation rate would be

Figure 3. Morlet wavelet analysis of time series, performed using the online software of Torrence and Compo at http://ion.researchsystems.com/IONScript/wavelet/ [*Torrence and Compo*, 1998]. (left) Top to bottom: V/Al, Mo/Al, U/Al, Ba/Al (LA-ICP-MS count ratios in PP44PC). (right) Top to bottom: log non-sea-salt K^+ in GISP2 [*Mayewski et al.*, 1997], residual $\delta^{14}C$ around a 2000 year running mean of the IntCal04 calibration line [*Reimer et al.*, 2004], $\delta^{18}O_{calcite}$ of Qunf Cave stalagmite Q5 in southern Oman [*Fleitmann et al.*, 2003]. All series were low-pass filtered at a cutoff of 30 years, detrended within the interval presented and normalized to unit variance prior to analysis. Wavelet power is scaled by the global wavelet spectrum (to the right of each plot). The cross-hatched region is the cone of influence, where zero padding has reduced the variance. The thick solid line contour is the 10% significance level, using a red noise (autoregressive lag 1) background spectrum. This 10% significance level is represented in the global wavelet power spectra by the dashed line. Note that the significance level is arbitrary and zones of high spectral power discussed in the text may fall outside the significance threshold. Horizontal dashed lines divide wavelet spectra into arbitrary 30–100 year, 100–300 year, and 300–600 year bands.

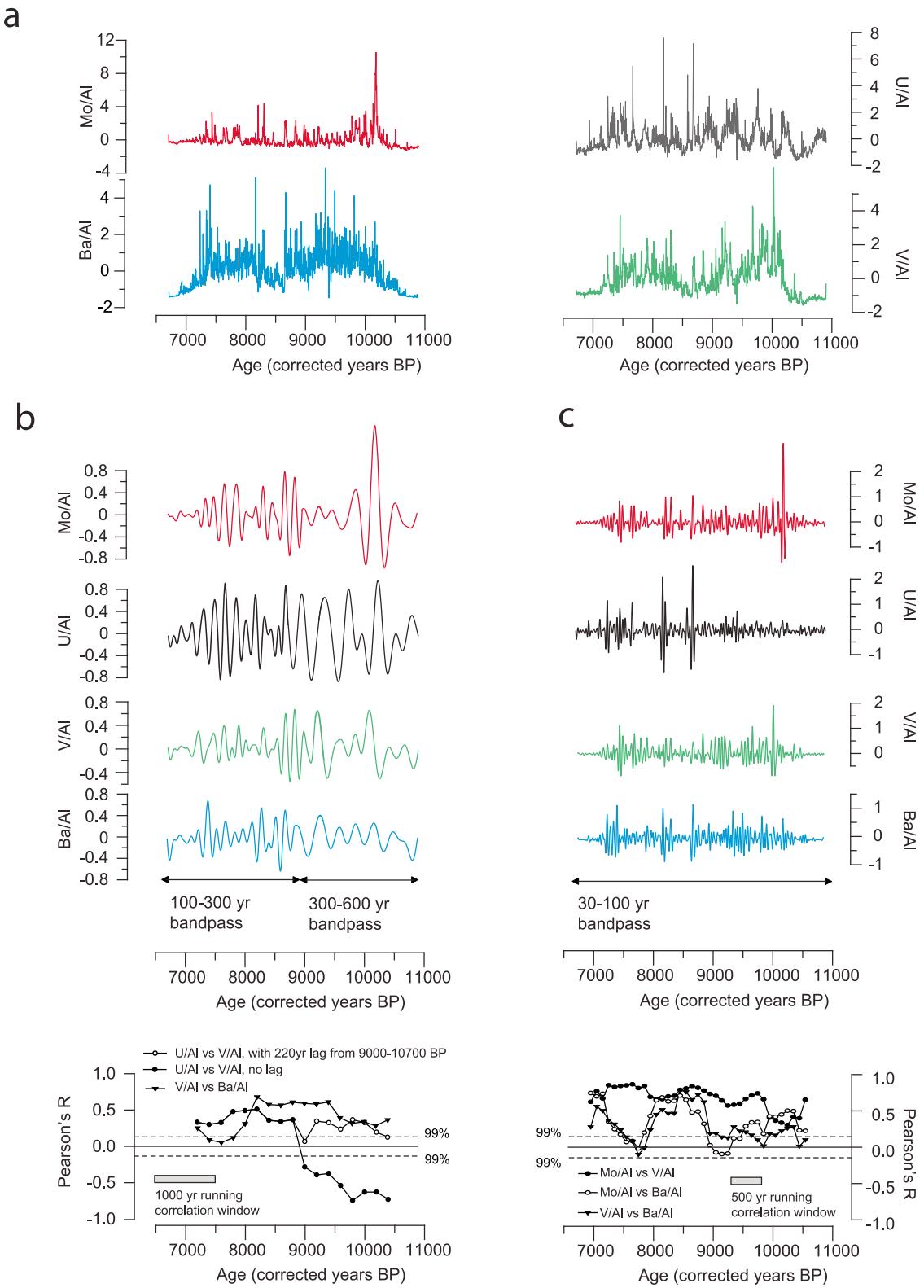
a
Mo/Al
Ba/Al
U/Al
V/Al
Age (corrected years BP)
b
c
100-300 yr bandpass
300-600 yr bandpass
30-100 yr bandpass
U/Al vs V/Al, with 220yr lag from 9000-10700 BP
U/Al vs V/Al, no lag
V/Al vs Ba/Al
Pearson's R
99%
1000 yr running correlation window
Mo/Al vs V/Al
Mo/Al vs Ba/Al
V/Al vs Ba/Al
500 yr running correlation window

Figure 4

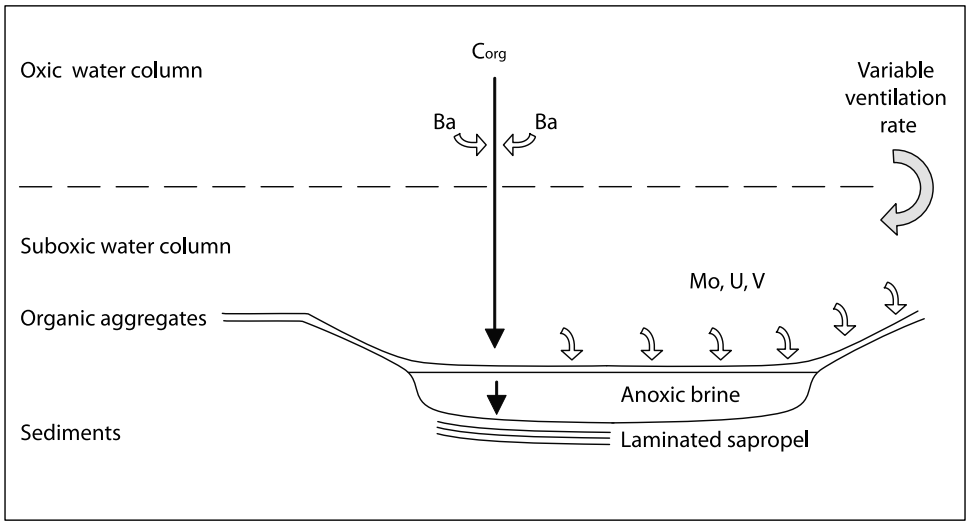

Figure 5. Schematic representation of mechanisms responsible for sedimentary enrichment during sapropel S1 of the elements investigated in this study. Ba precipitates as biogenic barite in descending organic matter, and organic aggregates accumulate at the seawater-brine interface. Severity of reducing conditions in deep waters controls rate of uptake of dissolved Mo, U, and V into organic aggregates, resulting in similar enrichments in brine and nonbrine sediments. Severity of reducing conditions is controlled by the organic matter flux and the rate of ventilation of deep waters. Ongoing anoxia in the brine environment after sapropel deposition preserves enrichments within the brine basin.

expected to generate constant ambient redox conditions, and thus a constant *potential* enrichment rate of trace metals (assuming no basin reservoir effect), leaving the *observed* enrichment rate sensitive to changes in the organic carbon flux. Conversely, high variability in the ventilation rate leads to fluctuating ambient redox conditions, which overprint the influence of the carbon flux on observed trace metal enrichments. Modeling studies estimate generally lower ventilation rates during S1 compared to today [*Myers et al.*, 1998], indicating that reduced ventilation most likely played a role in determining deep-water redox conditions. On the other hand, ongoing ventilation of some degree is implied by the periodical presence of oxyphilic benthic foraminifera in the Aegean Sea and offshore Libya throughout S1 [*Casford et al.*, 2003]. Both concepts are compatible with our trace metal enrichment data, which evoke a model of generally reduced, though highly variable, ventilation rate of the eastern Mediterranean during S1.

4.6. Element-Specific Enrichment Characteristics

[22] The in-phase Mo/Al, U/Al and V/Al variability in the 100–300 year band pass during late S1 suggests that, in this interval, all three elements responded similarly to ventilation rate changes, with peak enrichments occurring at times of minimum water column E_h. Closer inspection of the raw profiles (Figure 4a) shows that the 100–300 year U/Al peaks are generally broader than those in V/Al, and V/Al peaks broader than those in Mo/Al. This implies that the onset of precipitation of the three metals during individual "stagnation" events occurred in the sequence U → V → Mo (see Figure 1a), supporting the commonly held perception of enhanced sedimentary U as an indicator of mildly reducing conditions [e.g., *Arnaboldi and Meyers*, 2007; *Gallego-Torres et al.*, 2010; *Hendy and Pedersen*, 2005]. The sensitive response of U enrichment to decreasing E_h also explains the generally lower frequency of the U/Al signal compared to V and Mo. In contrast, the abrupt onset and termination of Mo/Al peaks force power in the wavelet spectrum toward the higher frequencies (Figure 3). These sharp peaks most likely reflect activation of the so-called "sulfide switch" [*Helz et al.*, 1996], in which a critical concentration of free HS^- greatly accelerates the rate of Mo precipitation by generation of particle-reactive oxythiomolybdates.

[23] Assuming similar basic mechanisms to control the enrichments during early S1, the negative coherence between U/Al and V/Al in the 300–600 year band pass of this interval

Figure 4. (a) Detrended, normalized LA-ICP-MS Element/Al data used as input for subsequent band-pass filtering. (b) LA-ICP-MS Element/Al data, band-pass filtered at 300–600 years from 10700 to 9000 years B.P. and at 100–300 years from 9000 to 6700 years B.P., and running correlation analysis of selected pairs of series. Each data point represents the magnitude of Pearson's R for the linear correlation between two series, within a 1000 year window centered on the data point. Note that the 99% confidence threshold is sensitive to the resolution of resampling during detrending and normalization of data (2 years). (c) LA-ICP-MS Element/Al data, band-pass filtered at 30–100 years from 10700 to 6700 years B.P., and running correlation analysis of selected pairs of series. Each data point represents the magnitude of Pearson's R for the correlation between two series, within a 500 year window centered on the data point. Note that the 99% confidence threshold is sensitive to the resolution of resampling during detrending and normalization of data (2 years).

is unexpected. However, the two series show a strong positive coherence if a 220 year lag is applied to the V/Al data prior to the running correlation analysis (Figure 4b). One explanation of this apparent phase lag is that the deep-water dissolved uranium concentration decreased during the longer stagnation cycles of early S1 (relative to late S1), decreasing the precipitation flux despite the ongoing low-E_h conditions. In other words, the U flux displays an eastern Mediterranean-wide basin reservoir effect [*Algeo and Lyons*, 2006]. As a consequence, the maximum U flux in each stagnation occurred some ~220 years prior to the timing of minimum E_h, after which the flux declined until increased ventilation again recharged the deep-water U reservoir. Thus, although U/Al appears to be the most sensitive recorder of the onset of individual stagnations, V/Al and Mo/Al may be more reliable indicators of the timing of minimum E_h.

4.7. Climate Control on Ventilation and Export Productivity During S1

[24] The LA-ICP-MS data from PP44PC provide a high-resolution counterpart to a number of existing records, which may be used to investigate the potential climatic controls on the observed variability in export productivity and redox conditions during S1 (Figure 3). Variable incident solar radiation has been postulated as the ultimate driver of multicentennial climate variability in the Holocene [*Bond et al.*, 2001; *Fleitmann et al.*, 2003; *Lamy et al.*, 2006], and is represented by the tree-ring-based $\delta^{14}C_{residual}$ time series. The record of non-sea-salt K^+ in the GISP2 ice core [*Mayewski et al.*, 1997] has been proposed to reflect the strength of the Siberian anticyclone, which in turn influences winter wind patterns in the Aegean Sea region [*Rohling et al.*, 2002b]. In contrast, the Qunf Cave $\delta^{18}O_{calcite}$ record [*Fleitmann et al.*, 2003, 2007] represents the mean latitude and intensity of summer monsoon precipitation on the Arabian peninsula. These three records have been selected for comparison with our data specifically because of their high resolution, and regional to global significance as climate archives.

[25] A distinguishing feature of the $\delta^{14}C_{residual}$ record during the S1 interval is the presence of spectral power in the 300–600 year band from ~10700–8500 B.P. (roughly corresponding to early S1) and the absence of such power during late S1 (Figure 3). In contrast, power in the 100–300 year and 30–100 year bands persists throughout S1 (note that frequency variability in $\delta^{14}C_{residual}$ is not related to changes in sampling resolution of this record, since existing tree ring archives extend to 12.4 kyr B.P.). *Fleitmann et al.* [2003] presented a visual comparison of the $\delta^{14}C_{residual}$ and Qunf Cave $\delta^{18}O_{calcite}$ records, suggesting that the intensity of monsoonal precipitation was sensitive to incident solar radiation during the interval corresponding to early S1. Our wavelet analysis supports this interpretation; elevated power in the 300–600 year band is also present in Qunf Cave $\delta^{18}O_{calcite}$ during early S1, but absent in late S1 (Figure 3). Furthermore, a similar (though less pronounced) concentration of power in the 300–600 year band during early S1 is observed in the non-sea-salt K^+ record from GISP2 (Figure 3). These observations imply a degree of connectivity between tropical and extratropical climate variability during S1, with variable solar irradiance as the driving force.

[26] The pronounced variability in our LA-ICP-MS records indicates that the intensity of sapropel conditions, as measured by export productivity and redox conditions at the seawater-brine interface of the Urania basin, fluctuated greatly on multidecadal to multicentennial time scales. The similarity of the U/Al and V/Al wavelet spectra with that of the $\delta^{14}C_{residual}$ record, namely, the presence of strong 300–600 year variability during early S1 and more dominant 100–300 year variability during late S1, suggests that ventilation of the eastern Mediterranean during S1 may have been controlled by global climate variability. However, such a control may have proceeded by a number of mechanisms. On the one hand, the link between enhanced runoff from north Africa and sapropel conditions is well established [e.g., *Rossignol-Strick et al.*, 1982; *Rossignol-Strick*, 1985; *Rohling et al.*, 2002a]. Assuming Qunf Cave $\delta^{18}O_{calcite}$ to approximate monsoon intensity across the wider north African continent, variable ventilation of the eastern Mediterranean during S1 may thus be coupled to variable runoff from north Africa. On the other hand, modeling results suggest that antiestuarine circulation of the Mediterranean persisted throughout S1 [*Rohling*, 1994; *Myers et al.*, 1998], implying that deep-water formation occurred, as today, in the Adriatic and Aegean Seas [*Pinardi and Masetti*, 2000]. Hence, variable severity of winter cooling in these northern subbasins, as recorded by GISP2 non-sea-salt K^+, may also have influenced ventilation of the eastern Mediterranean during S1 [see *Rohling et al.*, 2002b]. As a third possibility, local climate patterns such as the Mediterranean monsoon [*Arz et al.*, 2003] may have responded directly to variability in solar irradiance.

[27] If the enrichments of redox-sensitive trace metals were indeed climate controlled, the generally positive coherence of Ba/Al with V/Al (Figures 4b and 4c) implies that export productivity was also sensitive to climate variability on multidecadal to multicentennial time scales. This may be expected if the hydrographic rearrangements controlling ventilation also influenced the magnitude of the deep-chlorophyll maximum [*Rohling and Gieskes*, 1989] and the flux of mat-forming diatoms from the photic zone [*Kemp et al.*, 1999]. However, the coherence of Ba/Al with V/Al in each band pass is clearly much weaker during fully developed sapropel conditions in both early S1 and late S1 (Figures 4b and 4c), suggesting that export productivity became less sensitive to climate variability as S1 became more intense. Higher-amplitude variability in the ventilation rate may be partly responsible for the observed decoupling of the Ba enrichment from those of Mo, U and V, but this in itself does not explain why export productivity did not respond simultaneously to climate oscillations. We suggest that internal feedback mechanisms sustaining the supply of nutrients to the photic zone [*Sachs and Repeta*, 1999; *Slomp et al.*, 2002] may have responded in a nonlinear way to climate forcing, decoupling export productivity from climate variability on multidecadal to multicentennial time scales.

5. Conclusions

[28] The anoxic, hypersaline Urania basin in the deep eastern Mediterranean provides a unique recorder of high-

resolution variability in sediment geochemistry during sapropel S1. Density stratification between the brine in the basin and the overlying seawater ensures that anoxia and high salinity prevailed, at least since S1 deposition and possibly before, protecting enrichments of barite and redox-sensitive trace elements (Mo, U, V) from remobilization. Sedimentary Ba is enriched well above detrital values and correlates strongly with organic carbon, implying biogenic barite to be the dominant Ba phase and hence permitting the use of Ba/Al as a proxy for export productivity. Redox-sensitive trace metal precipitation is shown to have taken place most likely near the seawater-brine interface, under the direct influence of deep-water redox conditions. The sedimentary enrichments of these metals thus provide a record of redox conditions in the deep waters of the eastern Mediterranean during S1. LA-ICP-MS scanning reveals strong multidecadal to multicentennial variability in the sedimentary enrichments of all four elements. A switch in the dominant period of variability in redox-sensitive trace metal enrichment, from 300 to 600 years during early S1 to 100–300 years during late S1, is interpreted to represent a climate-driven change in the rate of ventilation of the eastern Mediterranean. Enrichment of Ba is partially decoupled from this pattern during fully developed sapropel conditions, implying an alternative control on export productivity at these times.

[29] **Acknowledgments.** The cores used in this work were recovered during the PASS2 project. Shipboard crews are acknowledged for their assistance. PASS2, and the subsequent research, was supported by the Dutch Organisation for Scientific Research (NWO). Helen de Waard and Gijs Nobbe are thanked for analytical assistance at the University of Utrecht. Discussions with the reading committee in association with the Ph.D. defense of Tom Jilbert contributed to the final outcome. Thomas Algeo and an anonymous reviewer are thanked for detailed comments which greatly improved the manuscript.

References

Algeo, T. J., and T. W. Lyons (2006), Mo-total organic carbon covariation in modern anoxic marine environments: Implications for analysis of paleoredox and paleohydrographic conditions, *Paleoceanography*, *21*, PA1016, doi:10.1029/2004PA001112.

Arnaboldi, M., and P. A. Meyers (2007), Trace element indicators of increased primary production and decreased water-column ventilation during deposition of latest Pliocene sapropels at five locations across the Mediterranean Sea, *Palaeogeogr. Palaeoclimatol. Palaeoecol.*, *249*, 425–443, doi:10.1016/j.palaeo.2007.02.016.

Arz, H. W., F. Lamy, J. Pätzold, P. Müller, and M. Prins (2003), Mediterranean moisture source for an Early Holocene humid period in the northern Red Sea, *Science*, *300*, 118–121, doi:10.1126/science.1080325.

Bale, C. W., P. Chartrand, S. A. Degtrev, G. Eriksson, K. Hack, R. Ben Mahfoud, J. Melancon, A. D. Pelton, and S. Petersen (2002), FactSage thermochemical software and databases, *Calphad*, *26*, 189–228, doi:10.1016/S0364-5916(02)00035-4.

Bard, E., G. Delaygue, F. Rostek, F. Antonioli, S. Silenzi and D. P. Schrag (2002), Hydrological conditions over the western Mediterranean basin during the deposition of the cold Sapropel 6 (ca. 175 kyr BP), *Earth Planet. Sci. Lett.*, *202*, 481–494. doi:10.1016/S0012-821X(02)00788-4.

Bar-Matthews, M., A. Ayalon, M. Gilmour, A. Matthews, and C. J. Hawkeswort (2003), Sea-land oxygen isotopic relationships from planktonic foraminifera and speleothems in the eastern Mediterranean region and their implication for paleorainfall during interglacial intervals, *Geochim. Cosmochim. Acta*, *67*(17), 3181–3199, doi:10.1016/S0016-7037(02)01031-1.

Bishop, J. K. B. (1988), The barite-opal-organic carbon association in oceanic particulate matter, *Nature*, *332*, 341–343, doi:10.1038/332341a0.

Boldrin, A., and S. Rabitti (1990), Hydrography of the brines in the Bannock and Tyro anoxic basins (eastern Mediterranean), *Mar. Chem.*, *31*, 21–33, doi:10.1016/0304-4203(90)90029-C.

Bond, G., B. Kromer, J. Beer, R. Muscheler, M. N. Evans, W. Showers, S. Hoffmann, R. Lotti-Bond, I. Hajdas, and G. Bonani (2001), Persistent solar influence on north Atlantic climate during the Holocene, *Science*, *294*, 2130–2136, doi:10.1126/science.1065680.

Brumsack, H. J. (2006), The trace metal content of recent organic carbon-rich sediments: Implications for Cretaceous black shale formation, *Palaeogeogr. Palaeoclimatol. Palaeoecol.*, *232*, 344–361, doi:10.1016/j.palaeo.2005.05.011.

Calvert, S. E. (1983), Geochemistry of Pleistocene sapropels and associated sediments from the eastern Mediterranean, *Oceanol. Acta*, *6*, 255–267.

Camerlenghi, A. (1990), Anoxic basins of the eastern Mediterranean: Geological framework, *Mar. Chem.*, *31*, 1–19, doi:10.1016/0304-4203(90)90028-B.

Casford, J. S. L., E. J. Rohling, R. H. Abu-Zied, C. Fontanier, F. J. Jorissen, M. J. Leng, G. Schmiedl, and J. Thomson (2003), A dynamic concept for eastern Mediterranean circulation and oxygenation during sapropel formation, *Palaeogeogr. Palaeoclimatol. Palaeoecol.*, *190*, 103–119, doi:10.1016/S0031-0182(02)00601-6.

Cita, M. B., and D. Grignani (1982), Nature and origin of Late Neogene Mediterranean sapropels, in *Nature and origin of Cretaceous carbon-rich facies*, edited by S. O. Schlanger and M. B. Cita, pp. 165–196, Academic, San Diego, Calif.

Colodner, D., J. Edmond, and E. Boyle (1995), Rhenium in the Black Sea: Comparison with molybdenum and uranium, *Earth Planet. Sci. Lett.*, *131*, 1–15. doi:10.1016/0012-821X(95)00010-A.

Crusius, J., S. Calvert, T. Pedersen and D. Sage (1996), Rhenium and molybdenum enrichments in sediments as indicators of oxic, suboxic and sulphidic conditions of deposition, *Earth Planet. Sci. Lett.*, *145*, 65–78. doi:10.1016/S0012-821X(96)00204-X.

de Lange, G. J., and H. L. ten Haven (1983), Recent sapropel formation in the eastern Mediterranean, *Nature*, *305*, 797–798, doi:10.1038/305797a0.

de Lange, G. J., G. Catalano, G. P. Klinkhammer, and G. W. Luther (1990a), The interface between oxic seawater and the anoxic Bannock Brine; its sharpness and the consequences for the redox-related cycling of Mn and Ba, *Mar. Chem.*, *31*, 205–217, doi:10.1016/0304-4203(90)90039-F.

de Lange, G. J., J. J. Middelburg, C. H. van der Weijden, G. Catalano, G. W. Luther III, D. J. Hydes, J. R. W. Woittiez, and G. P. Klinkhammer (1990b), Composition of anoxic hypersaline brines in the Tyro and Bannock Basins, eastern Mediterranean, *Mar. Chem.*, *31*, 63–88, doi:10.1016/0304-4203(90)90031-7.

de Lange, G. J., J. Thomson, A. Reitz, C. P. Slomp, M. S. Principato, E. Erba, and C. Corselli (2008), Synchronous basin-wide formation and redox-controlled preservation of a Mediterranean sapropel, *Nat. Geosci.*, *1*, 606–610, doi:10.1038/ngeo283.

Dehairs, F., R. Chesselet, and J. Jedwab (1980), Discrete suspended particles of barite and the barium cycle in the open ocean, *Earth Planet. Sci. Lett.*, *49*(2), 528–550. doi:10.1016/0012-821X(80)90094-1.

Dymond, J., E. Suess, and M. Lyle (1992), Barium in deep-sea sediment: A geochemical proxy for paleoproductivity, *Paleoceanography*, *7*(2), 163–181, doi:10.1029/92PA00181.

Eagle, M., A. Paytan, K. R. Arrigo, G. van Dijken, and R. W. Murray (2003), A comparison between excess barium and barite as indicators of carbon export, *Paleoceanography*, *18*(1), 1021, doi:10.1029/2002PA000793.

Emerson, S. R., and S. S. Huested (1991), Ocean anoxia and the concentrations of molybdenum and vanadium in seawater, *Mar. Chem.*, *34*, 177–196, doi:10.1016/0304-4203(91)90002-E.

Fleitmann, D., S. J. Burns, M. Mudelsee, U. Neff, J. Kramers, A. Mangini, and A. Matter (2003), Holocene Forcing of the Indian Monsoon Recorded in a Stalagmite from southern Oman, *Science*, *300*, 1737–1739, doi:10.1126/science.1083130.

Fleitmann, D., et al. (2007), Holocene ITCZ and Indian monsoon dynamics recorded in stalagmites from Oman and Yemen (Socotra), *Quat. Sci. Rev.*, *26*, 170–188, doi:10.1016/j.quascirev.2006.04.012.

Gallego-Torres, D., F. Martinez-Ruiz, G. J. de Lange, F. J. Jimenez-Espejo, and M. Ortega-Huertas (2010), Trace-elemental derived paleoceanographic and paleoclimatic conditions for Pleistocene eastern Mediterranean sapropels,

Palaeogeogr. Palaeoclimatol. Palaeoecol., *293*, 76–89, doi:10.1016/j.palaeo.2010.05.001.

Helz, G. R., C. V. Miller, J. M. Charnock, J. F. W. Mosselmans, R. A. Pattrick, C. D. Garner, and D. J. Vaughan (1996), Mechanism of molybdenum removal from the sea and its concentration in black shales: EXAFS evidence, *Geochim. Cosmochim. Acta*, *60*, 3631–3642, doi:10.1016/0016-7037(96)00195-0.

Hendy, I. L., and T. F. Pedersen (2005), Is pore water oxygen content decoupled from productivity on the California Margin? Trace element results from Ocean Drilling Program Hole 1017E, San Lucia slope, California, *Paleoceanography*, *20*, PA4026, doi:10.1029/2004PA001123.

Henneke, E., and G. J. de Lange (1990), The distribution of DOC and POC in the water column and brines of the Tyro and Bannock basins, *Mar. Chem.*, *31*, 113–122, doi:10.1016/0304-4203(90)90033-9.

Hilgen, F. J. (1991), Astronomical calibration of Gauss to Matuyama sapropels in the Mediterranean and implication for the geomagnetic polarity time scale, *Earth Planet. Sci. Lett.*, *104*, 226–244. doi:10.1016/0012-821X(91)90206-W.

Hübner, A., G. J. de Lange, J. Dittmer, and P. Halbach (2003), Geochemistry of an exotic sediment layer above sapropel S-1: Mud expulsion from the Urania Basin, eastern Mediterranean?, *Mar. Geol.*, *197*, 49–61, doi:10.1016/S0025-3227(03)00085-9.

Hughen, K. A., et al. (2004), Marine04 marine radiocarbon age calibration, 0–26 cal kyr BP, *Radiocarbon*, *46*, 1059–1086.

Jilbert, T., G. J. de Lange, and G.-J. Reichart (2008), Fluid displacive resin embedding of laminated sediments: Preserving trace metals for high-resolution palaeoclimate investigations, *Limnol. Oceanogr. Methods*, *6*, 16–22.

Kastens, K. A. (1981), Structural causes and sedimentological effects of the 'cobblestone topography' in the eastern Mediterranean, Ph. D. dissertation, Scripps Inst. of Oceanogr., Univ. of Calif., San Diego.

Kemp, A. E. S., R. B. Pearce, I. Koizumi, J. Pike, and S. J. Rance (1999), The role of mat-forming diatoms in the formation of Mediterranean sapropels, *Nature*, *398*, 57–61, doi:10.1038/18001.

Klinkhammer, G. P., and M. R. Palmer (1991), Uranium in the oceans - where it goes and why, *Geochim. Cosmochim. Acta*, *55*, 1799–1806, doi:10.1016/0016-7037(91)90024-Y.

Kotthoff, U., J. Pross, U. C. Muller, O. Peyron, G. Schmiedl, H. Schulz, and A. Bordon (2008), Climate dynamics in the borderlands of the Aegean Sea during formation of sapropel S1 deduced from a marine pollen record, *Quat. Sci. Rev.*, *27*, 832–845, doi:10.1016/j.quascirev.2007.12.001.

Lamy, F., H. W. Arz, G. C. Bond, A. Bahr, and J. Pätzold (2006), Multicentennial-scale hydrological changes in the Black Sea and northern Red Sea during the Holocene and the Arctic/North Atlantic Oscillation, *Paleoceanography*, *21*, PA1008, doi:10.1029/2005PA001184.

Laws, E. A., P. G. Falkowski, W. O. Smith, H. Ducklow, and J. J. McCarthy (2000), Temperature effects on export production in the open ocean, *Global Biogeochem. Cycles*, *14*, 1231–1246, doi:10.1029/1999GB001229.

Lourens, L. J., A. Antonarakou, F. J. Hilgen, A. A. M. van Hoof, C. Vergnaud-Grazzini, and W. J. Zachariasse (1996), Evaluation of the Plio-Pleistocene astronomical timescale, *Paleoceanography*, *11*, 391–413, doi:10.1029/96PA01125.

Mayewski, P. A., L. D. Meeker, M. S. Twickler, S. I. Whitlow, Q. Yang, W. B. Lyons, and M. Prentice (1997), Major features and forcing of high-latitude northern hemisphere atmospheric circulation using a 110,000-year-long glaciochemical series, *J. Geophys. Res.*, *102*, 26,345–26,366, doi:10.1029/96JC03365.

McManus, J., et al. (1998), Geochemistry of barium in marine sediments: Implications for its use as a paleoproxy, *Geochim. Cosmochim. Acta*, *62*(21–22), 3453–3473, doi:10.1016/S0016-7037(98)00248-8.

Mercone, D., J. Thomson, R. H. Abu-Zied, I. W. Croudace, and E. J. Rohling (2001), High-resolution geochemical and micropalaeontological profiling of the most recent eastern Mediterranean sapropel, *Mar. Geol.*, *177*, 25–44, doi:10.1016/S0025-3227(01)00122-0.

Meyers, P. A., and M. Arnaboldi (2005), Trans-Mediterranean comparison of geochemical paleoproductivity proxies in a mid-Pleistocene interrupted sapropel, *Palaeogeogr. Palaeoclimatol. Palaeoecol.*, *222*, 313–328, doi:10.1016/j.palaeo.2005.03.020.

Myers, P. G., K. Haines, and E. J. Rohling (1998), Modeling the paleocirculation of the Mediterranean: The last glacial maximum and the Holocene with emphasis on the formation of sapropel S-1, *Paleoceanography*, *13*, 586–606, doi:10.1029/98PA02736.

Nijenhuis, I. A., H-J. Bosch, J. S. Sinninghe Damsté, H-J. Brumsack and G. J. de Lange (1999), Organic matter and trace metal rich sapropels and black shales: A geochemical comparison, *Earth Planet. Sci. Lett.*, *169*, 277–290. doi:10.1016/S0012-821X(99)00083-7.

Olausson, E. (1961), Studies of deep sea cores, *Reports of the Swedish deep sea expedition 1947–1948*, *8*, 353–391.

Passier, H. F., H. J. Bosch, I. A. Nijenhuis, L. J. Lourens, M. E. Böttcher, A. Leenders, J. S. Sinninghe Damste, G. J. de Lange, and J. W. de Leeuw (1999), Sulphidic Mediterranean surface waters during Pliocene sapropel formation, *Nature*, *397*, 146–149, doi:10.1038/16441.

Paytan, A., and E. M. Griffith (2007), Marine barite: Recorder of variations in ocean export productivity, *Deep Sea Res., Part II*, *54*, 687–705, doi:10.1016/j.dsr2.2007.01.007.

Pinardi, N., and E. Masetti (2000), Variability of the large scale general circulation of the Mediterranean Sea from observations and modelling: A review, *Palaeogeogr. Palaeoclimatol. Palaeoecol.*, *158*, 153–173, doi:10.1016/S0031-0182(00)00048-1.

Pruysers, P. A., G. J. de Lange, and J. J. Middelburg (1991), Geochemistry of eastern Mediterranean sediments: Primary sediment composition and diagenetic alterations, *Mar. Geol.*, *100*, 137–154, doi:10.1016/0025-3227(91)90230-2.

Reimer, P. J., et al. (2004), IntCal04 terrestrial radiocarbon age calibration, 0–26 cal kyr BP, *Radiocarbon*, *46*, 1029–1058.

Reitz, A., K. Pfeifer, G. J. de Lange, and J. Klump (2004), Biogenic barium and the detrital Ba/Al ratio: A comparison of their direct and indirect determination, *Mar. Geol.*, *204*, 289–300, doi:10.1016/S0025-3227(04)00004-0.

Reitz, A., J. Thomson, G. J. de Lange, and C. Hensen (2006), Source and development of large manganese enrichments above eastern Mediterranean sapropel S1, *Paleoceanography*, *21*, PA3007, doi:10.1029/2005PA001169.

Rohling, E. J. (1994), Review and new aspects concerning the formation of eastern Mediterranean sapropels, *Mar. Geol.*, *122*, 1–28, doi:10.1016/0025-3227(94)90202-X.

Rohling, E. J., and H. L. Bryden (1994), A method for estimating past changes in the eastern Mediterranean freshwater budget, using reconstructions of sea level and hydrography, *Proc. K. Ned. Akad. Wet. Biol. Chem. Geol. Phys. Med. Sci.*, *97*, 201–217.

Rohling, E. J., and W. W. C. Gieskes (1989), Late Quaternary changes in Mediterranean intermediate water density and formation rate, *Paleoceanography*, *4*, 531–545, doi:10.1029/PA004i005p00531.

Rohling, E. J., and F. J. Hilgen (1991), The eastern Mediterranean climate at times of sapropel formation—A review, *Geol. Mijnbouw*, *70*, 253–264.

Rohling, E. J., T. R. Cane, S. Cooke, M. Sprovieri, I. Bouloubassi, K. C. Emeis, R. Schiebel, D. Kroon, F. J. Jorissen, A. Lorre, and A. E. S. Kemp (2002a), African monsoon variability during the previous interglacial maximum, *Earth Planet. Sci. Lett.*, *202*, 61–75. doi:10.1016/S0012-821X(02)00775-6.

Rohling, E. J., P. A. Mayewski, R. H. Abu-Zied, J. S. L. Casford, and A. Hayes (2002b), Holocene atmosphere-ocean interactions: Records from Greenland and the Aegean Sea, *Clim. Dyn.*, *18*, 587–593, doi:10.1007/s00382-001-0194-8.

Rossignol-Strick, M. (1985), Mediterranean Quaternary sapropels, an intermediate response of the African monsoon to variation of insolation, *Palaeogeogr. Palaeoclimatol. Palaeoecol.*, *49*, 237–263, doi:10.1016/0031-0182(85)90056-2.

Rossignol-Strick, M., W. Nesteroff, P. Olive, and C. Vergnaud-Grazzini (1982), After the deluge: Mediterranean stagnation and sapropel formation, *Nature*, *295*, 105–110, doi:10.1038/295105a0.

Rutten, A., and G. J. de Lange (2003), Sequential extraction of iron, manganese and related elements in S1 sapropel sediments, eastern Mediterranean, *Palaeogeogr. Palaeoclimatol. Palaeoecol.*, *190*, 79–101, doi:10.1016/S0031-0182(02)00600-4.

Sachs, J. P., and D. J. Repeta (1999), Oligotrophy and nitrogen fixation during eastern Mediterranean sapropel events, *Science*, *286*, 2485–2488, doi:10.1126/science.286.5449.2485.

Sass, A. M., H. Sass, M. J. L. Coolen, H. Cypionka, and J. Overmann (2001), Microbial communities in the chemocline of a hypersaline deep-sea basin (Urania basin, Mediterranean Sea), *Appl. Environ. Microbiol.*, *67*(12), 5392–5402, doi:10.1128/AEM.67.12.5392-5402.2001.

Siani, G., M. Paterne, M. Arnold, E. Bard, B. Métivier, N. Tisnerat, and F. Bassinot (2000), Radiocarbon reservoir ages in the Mediterranean Sea, *Radiocarbon*, *42*(2), 271–280.

Siani, G., M. Paterne, E. Michel, R. Sulpizio, A. Sbrana, M. Arnold, and G. Haddad (2001), Mediterranean sea-surface radiocarbon reservoir age changes since the Last Glacial Maximum, *Science*, *294*, 1917–1920, doi:10.1126/science.1063649.

Slomp, C. P., J. Thomson, and G. J. de Lange (2002), Enhanced regeneration of phosphorus during formation of the most recent eastern Mediterranean sapropel (S1), *Geochim. Cosmochim. Acta*, *66*, 1171–1184, doi:10.1016/S0016-7037(01)00848-1.

Stenni, B., and A. Longinelli (1990), Stable isotope study of water, gypsum and carbonate samples from the Bannock and Tyro Basins, eastern Mediterranean, *Mar. Chem.*, *31*, 123–135, doi:10.1016/0304-4203(90)90034-A.

Takeno, N. (2005), Atlas of Eh-pH diagrams: Intercomparison of thermodynamic databases, *Geol. Surv. Jpn. Open File Rep. 419*, Tokyo.

Thomson, J., N. C. Higgs, T. R. S. Wilson, W. Croudace, G. J. de Lange, and P. J. M. van Santvoort (1995), Redistribution and geochemical behavior of redox-sensitive elements around S1, the most recent eastern Mediterranean sapropel, *Geochim. Cosmochim. Acta*, *59*, 3487–3501, doi:10.1016/0016-7037(95)00232-O.

Thunell, R. C., D. F. Williams, and P. R. Belyea (1984), Anoxic events in the Mediterranean Sea in relation to the evolution of late Neogene climates, *Mar. Geol.*, *59*, 105–134, doi:10.1016/0025-3227(84)90090-2.

Torrence, C. and G. P. Compo (1998), A practical guide to wavelet analysis, *Bull. Am. Meteorol. Soc.*, *79*(1), 61–78, doi:10.1175/15200477(1998)079<0061:APGTWA>2.0.CO;2.

Tribovillard, N., V. Bout-Roumazeilles, T. Algeo, T. W. Lyons, T. Sionneau, J. C. Montero-Serrano, A. Riboulleau, and F. Baudin (2008), Paleodepositional conditions in the Orca Basin as inferred from organic matter and trace metal contents, *Mar. Geol.*, *254*(1–2), 62–72, doi:10.1016/j.margeo.2008.04.016.

Tribovillard, N., V. Bout-Roumazeilles, T. Sionneau, J. C. Montero-Serrano, A. Riboulleau, and F. Baudin (2009), Does a strong pycnocline impact organic-matter preservation and accumulation in an anoxic setting? The case of the Orca Basin, Gulf of Mexico, *C. R. Geosci.*, *341*(1), 1–9, doi:10.1016/j.crte.2008.10.002.

Turekian, K. K., and K. H. Wedepohl (1961), Distribution of the elements in some major units of the Earth's crust, *Geol. Soc. Am. Bull.*, *72*, 175–192, doi:10.1130/0016-7606(1961)72[175:DOTEIS]2.0.CO;2.

van der Weijden, C. H., J. J. Middelburg, G. J. de Lange, H. A. van der Sloot, D. Hoede, and J. R. W. Woittiez (1990), Profiles of the redox-sensitive trace elements As, Sb, V, Mo and U in the Tyro and Bannock Basins (eastern Mediterranean), *Mar. Chem.*, *31*, 171–186, doi:10.1016/0304-4203(90)90037-D.

van der Weijden, C. H., G. J. Reichart, and B. J. H. van Os (2006), Sedimentary trace element records over the last 200 kyr from within and below the northern Arabian Sea oxygen minimum zone, *Mar. Geol.*, *231*, 69–88, doi:10.1016/j.margeo.2006.05.013.

van der Wielen, P. W., et al. (2005), The enigma of prokaryotic life in deep hypersaline anoxic basins, *Science*, *307*, 121–123, doi:10.1126/science.1103569.

van Os, B. J. H., J. J. Middelburg, and G. J. de Lange (1991), Possible diagenetic mobilisation of barium in sapropelic sediment from the eastern Mediterranean: Anoxic basins and sapropel deposition in the eastern Mediterranean: Past and present, *Mar. Geol.*, *100*, 125–136, doi:10.1016/0025-3227(91)90229-W.

van Santvoort, P. J. M., G. J. de Lange, J. Thomson, H. Cussen, T. R. S. Wilson, M. D. Krom, and K. Ströhle (1996), Active post-depositional oxidation of the most recent sapropel (S1) in sediments of the eastern Mediterranean Sea, *Geochim. Cosmochim. Acta*, *60*, 4007–4024, doi:10.1016/S0016-7037(96)00253-0.

Vengosh, A., G. J. de Lange, and A. Starinsky (1998), Boron isotope and geochemical evidence for the origin of Urania and Bannock brines at the eastern Mediterranean: Effect of water-rock interactions, *Geochim. Cosmochim. Acta*, *62*, 3221–3228, doi:10.1016/S0016-7037(98)00236-1.

Wanty, R. B., and M. B. Goldhaber (1992), Thermodynamics and kinetics of reactions involving vanadium in natural systems – accumulation of vanadium in sedimentary rocks, *Geochim. Cosmochim. Acta*, *56*, 1471–1483, doi:10.1016/0016-7037(92)90217-7.

Warning, B., and H. J. Brumsack (2000), Trace metal signatures of eastern Mediterranean sapropels, *Palaeogeogr. Palaeoclimatol. Palaeoecol.*, *158*, 293–309, doi:10.1016/S0031-0182(00)00055-9.

G. J. de Lange, T. Jilbert, P. Mason, and G.-J. Reichart, Department of Earth Sciences–Geochemistry, Faculty of Geosciences, Utrecht University, PO Box 80.021, NL-3508 TA Utrecht, Netherlands. (jilbert@geo.uu.nl)